International Communications in Heat and Mass Transfer 58 (2014) 63–70

Contents lists available at ScienceDirect

International Communications in Heat and Mass Transfer

journal homepage: www.elsevier.com/locate/ichmt

# Effects of a porous medium on forced convection of a reciprocating curved channel☆

Wu-Shung Fu *, Chung-Jen Chen, Yu-Chih Lai, Shang-Hao Huang

*Department of Mechanical Engineering, National Chiao Tung University, Hsinchu 30010, Taiwan, ROC*

ARTICLE INFO

Available online 15 August 2014

*Keywords:*
Moving boundary problem
Porous medium
Forced convection
ALE method

ABSTRACT

Enhancement of heat transfer rates of a reciprocating curved channel partially installed by a porous medium is investigated numerically. The distribution of heat transfer rates on the heat surface of the reciprocating curved channel is rather non-uniform that easily causes a thermal damage to destroy the channel. A method of using the porous medium to enhance heat transfer rates of the channel is then developed to solve the thermal damage. The arbitrary Lagrangian–Eulerian method is firstly modified for treating a moving boundary problem of the porous medium. Main parameters of Reynolds numbers, porosities, frequencies and amplitudes are examined. The results show that the enhancements of heat transfer rates of most porous medium situations are achieved. However, heat transfer rates of a few porous medium situations are unexpectedly inferior to those of without porous medium situations.



## 1. Introduction

In order to fulfill a demand of lots of functions concentrated in a tiny device, heat loading of the device is then hugely increased. A topic for increasing heat transfer rates to decrease a damage caused by the huge heat generation of the device naturally becomes urgent and important. A porous medium, which is often used in solar cells, electric devices, heat exchangers, etc., possesses two characteristics of a thinly staggered and connected structure which provides a large convective heat transfer surface, and lots of connected porosities, which provide cooling fluids to flow through them freely to execute convective heat transfer with the structure. Unfortunately, the huge surface area of the porous medium usually results in severe drag resistance of cooling fluids. Therefore, the characteristics of the porous medium should be carefully taken into consideration for achieving enhancement of the heat transfer rates of heated devices by the porous medium.

In the past, lots of related literature investigated heat transfer mechanisms of the porous medium in situations of forced convection [1–15], mixed convection [16–21], natural convection [22–30], and obtained remarkable results. Heat generation devices mentioned in the above literature were fixed and not affected by dynamic motions. However, devices used in moving structures or portable equipment are difficult to avoid the influence of dynamic motions. Although lots of literature [31–36] investigated heat transfer mechanisms of the device subject to the reciprocating motion, which is a kind of dynamic motion and easily simulated, and clarified detailed phenomena. A method, which applies the porous medium to the device subject to the reciprocating motion for enhancing heat transfer rates, is not proposed yet, because the method needs to solve the effects of the reciprocating motion and porous medium on the heat transfer mechanism of the device simultaneously. It causes solution methods to be more complicated than those used in the above literature. Accordingly, related investigations are hardly conducted.

The aim of the study investigates the enhancement of heat transfer rates of a reciprocating curved channel partially installed by the porous medium numerically. The arbitrary Lagrangian–Eulerian method (ALE), which is firstly derived to be used in the porous medium, is adopted as the solution method to treat a moving boundary problem induced by the reciprocating curved channel. Parameters of the Reynolds numbers, porosities, frequencies and amplitudes are examined. The results show that the enhancements of heat transfer rates of most porous medium situations are achieved. In a few situations with the high porosity, heat transfer rates are unexpectedly inferior to those of without porous medium situations.

## 2. Physical model

A physical model of this study is a two dimensional curved channel which is composed of two vertical and one horizontal channels and is shown in Fig. 1. The total width and length are $w_1$ and $h_0$, respectively, and the width of the channel is $w_0$. A high and constant temperature $T_h$ is assigned on the top surface $\overline{BC}$, and the other surfaces are adiabatic. A porous medium is partially installed on the top surface in order to achieve heat transfer rates of the top surface. The height and porosity of the porous medium are $h_2$ and $\varepsilon$, respectively. Cooling fluids, of which the temperature and velocity are $T_0$ and $v_0$, respectively, via the left vertical channel flow into the curved channel. The region between

☆ Communicated by W.J. Minkowycz.

* Corresponding author at: Department of Mechanical Engineering, National Chiao Tung University, 1001 Ta Hsueh Road, Hsinchu 30056, Taiwan, ROC.
*E-mail address:* wsfu@mail.nctu.edu.tw (W.-S. Fu).

http://dx.doi.org/10.1016/j.icheatmasstransfer.2014.08.007
0735-1933/

**Nomenclature**

| | |
|---|---|
| Da | Darcy number (Da = $K/w_0^2$), Eq. (1) |
| $D_p$ | dimensionless diameter of a copper bead |
| e | element number in finite element method |
| *En* | enhancement factor for reciprocating motion of the channel, Eq. (27) |
| $f_C$ | dimensional reciprocating frequency of the horizontal channel ($s^{-1}$) |
| F | porous inertia factor used in momentum equation |
| $F_C$ | dimensionless reciprocating frequency of the horizontal channel |
| g | acceleration of gravity (m $s^{-2}$) |
| $h_0$ | dimensional height of the channel (m) |
| $h_1$ | dimensional height of the right vertical channel (m) |
| $h_2$ | dimensional height of the porous medium (m) |
| $k_e$ | equivalent thermal conductivity (W $m^{-1}$ $K^{-1}$) |
| $k_f$ | thermal conductivity of work fluid (W $m^{-1}$ $K^{-1}$) |
| *K* | permeability |
| $l_C$ | dimensional reciprocating amplitude of the horizontal channel (m) |
| $L_c$ | dimensionless reciprocating amplitude of the horizontal channel |
| m | number of non-linear iterations of the N–S equation |
| $Nu_{p,x}$ | local Nusselt number (porous medium), Eq. (24) |
| $\overline{Nu}_{p,x}$ | average Nusselt number (porous medium), Eq. (26) |
| $Nu_x$ | local Nusselt number (without porous medium), Eq. (23) |
| $\overline{Nu}$ | average Nusselt number (without porous medium), Eq. (25) |
| *p* | dimensional pressure (N $m^{-2}$) |
| P | dimensionless pressure |
| $P_P$ | dimensionless pressure of porous medium |
| Pr | Prandtl number ($=\rho c\upsilon/k_f$), Eq. (1) |
| $Pr_e$ | equivalent Prandtl number in porous medium ($=\rho c\upsilon/k_e$), Eq. (1) |
| $p_f$ | dimensional pressure of porous medium (N $m^{-2}$) |
| $p_\infty$ | dimensional reference pressure (N $m^{-2}$) |
| Re | Reynolds number ($=\rho_0\omega_0/\upsilon$), Eq. (1) |
| *RP* | ratio index of driving forces, Eq. (29) |
| *t* | dimensional time (s) |
| T | dimensional temperature (K) |
| $T_0$ | surrounding temperature (K) |
| $T_h$ | dimensional high temperature (K) |
| $T_p$ | dimensional temperature in porous medium |
| ΔT | temperature difference between $T_h$ and $T_0$ ($=T_h - T_0$) |
| *u*, *v* | dimensional velocities of *x*- and *y*- directions ($ms^{-1}$) |
| $u_p$, $v_p$ | dimensional velocities in porous medium ($ms^{-1}$) |
| U, V | dimensionless velocities of X- and Y- directions |
| $U_p$, $V_p$ | dimensionless velocities in porous medium ($ms^{-1}$) |
| $\left\vert\vec{U}\right\vert$ | dimensionless velocity magnitude ($=(U_p^2 + V_p^2)^{1/2}$) |
| $v_0$ | dimensional velocity of the inlet cooling air ($ms^{-1}$) |
| $V_0$ | dimensionless velocity of the inlet cooling air |
| $v_C$ | dimensional reciprocating velocity of the piston ($ms^{-1}$) |
| $V_C$ | dimensionless reciprocating velocity of the piston |
| $v_m$ | dimensional maximum velocity of the piston ($ms^{-1}$) |
| $V_m$ | dimensionless maximum velocity of the piston |
| $\hat{v}$ | dimensional mesh velocity in *y*- direction ($ms^{-1}$) |
| $\hat{V}$ | dimensionless mesh velocity in Y- direction |
| $V_\eta$ | dimensionless node velocity of the moving mesh region |
| $w_0$ | dimensional width of the channel (m) |
| $w_1$ | dimensional length of the horizontal channel (m) |
| *x*, *y* | dimensional Cartesian coordinates (m) |
| X, Y | dimensionless Cartesian coordinates |

*Greek symbols*

| | |
|---|---|
| υ | kinematic viscosity ($m^2$ $s^{-1}$) |
| α | thermal diffusivity ($m^2$ $s^{-1}$) |
| ε | porosity ($m^3$ $m^{-3}$) |
| τ | dimensionless time |
| Δτ | dimensionless time step interval |
| $\tau_P$ | dimensionless time interval of a periodic cycle |
| $\rho_0$ | dimensional density of air (kg $m^{-3}$) |
| $\rho_f$ | dimensional density of air in porous medium (kg $m^{-3}$) |
| $\eta_i$ | vertical position of the node in the moving mesh region |
| $\eta_0$ | vertical total length of the moving mesh region |
| θ | dimensionless temperature |
| $\theta_p$ | dimensionless temperature in porous medium |
| φ | dimensionless computational variables U, V and P |

*Superscripts*

| | |
|---|---|
| – | mean value |
| → | velocity vector |

*Subscripts*

| | |
|---|---|
| *f* | working fluid |
| *p* | porous medium |
| 0 | surroundings |

the $\overline{OP}$ and $\overline{MN}$ is flexible and can be elongated from $w_0$ to $w_0 + l_C$. The magnitude of $l_C$ is the reciprocating amplitude. Therefore, computational grids in this region are extensible. As the horizontal channel moves upward that means that the $\overline{MN}$ will be fixed and the $\overline{OP}$ to move upward, and the maximum moving distance is $l_C$. Afterward, the $\overline{OP}$ moves downward and returns to the original location. The moving velocity is $v_C$ expressed in terms of $v_C = v_m \sin(2\pi f_C t)$ in which $v_m$ and $f_C$ are the maximum velocity and frequency, respectively. The maximum velocity is equal to $2\pi l_C f_C$. The reciprocating motion of the channel affects behaviors of fluids transiently, thus phenomena become time-dependent and could be classified into a kind of moving boundary problem. For satisfying convergence criteria of computation processes, the length of the right vertical channel $h_1$ is long enough to hold fully developed conditions of temperature and velocity at the exit. For facilitating the analysis, the assumptions are described as follows:

(1) An incompressible laminar flow is adopted.
(2) Fluid properties are constant and the effect of the gravity is neglected.
(3) The no-slip condition is held on all surfaces. The fluid velocities on moving boundaries equal to the boundary moving velocities.
(4) The porous medium is made of spherical copper beads which do not chemically react with fluids.
(5) The transverse thermal dispersion is modeled by the Van Driest's wall function. The effective viscosity of the porous medium is equal to the viscosity of the fluids [9].

Based upon the characteristic scales of $w_0$, $v_0$, $\rho_0 v_0^2$ and $T_0$, the dimensionless variables are defined as follows

$$X = \frac{x}{w_0}, Y = \frac{y}{w_0}, U = \frac{u}{v_0}, V = \frac{v}{v_0}, V_C = \frac{v_C}{v_0}, U_p = \frac{u_p}{v_0}, V_p = \frac{v_p}{v_0}$$
$$P_p = \frac{p_f - p_\infty}{\rho_f v_0^2}, P = \frac{p - p_\infty}{\rho_0 v_0^2}, \tau = \frac{t v_0}{w_0}, \theta = \frac{T - T_0}{T_h - T_0}, \theta_p = \frac{T_p - T_0}{T_h - T_0}, Re = \frac{v_0 w_0}{\upsilon},$$
$$Pr = \frac{\rho c \upsilon}{k_f}, Pr_e = \frac{\rho c \upsilon}{k_e}, F_C = \frac{f_C w_0}{v_0}, Da = \frac{K}{w_0^2}, \left\vert\vec{U}\right\vert = \left(U_p^2 + V_p^2\right)^{1/2} \quad (1)$$

where $k\left(=\frac{\varepsilon^2 dp^2}{150(1-\varepsilon^2)}\right)$ is the permeability, and $k_e$ is the equivalent thermal conductivity of the porous medium and was derived from [9].

Based on the above dimensionless variables, governing equations for an internal flow, which includes the porous medium, and an external flow, which does not include the porous medium, can be separately derived as follows.

External flow:

Continuity equation

$$\frac{\partial U}{\partial X}+\frac{\partial V}{\partial Y}=0 \tag{2}$$

Momentum equations

X direction

$$\frac{\partial U}{\partial \tau}+U\frac{\partial U}{\partial X}+\left(V-\hat{V}\right)\frac{\partial U}{\partial Y}=-\frac{\partial P}{\partial X}+\frac{1}{Re}\left(\frac{\partial^2 U}{\partial X^2}+\frac{\partial^2 U}{\partial Y^2}\right) \tag{3}$$

Y direction

$$\frac{\partial V}{\partial \tau}+U\frac{\partial V}{\partial X}+\left(V-\hat{V}\right)\frac{\partial V}{\partial Y}=-\frac{\partial P}{\partial Y}+\frac{1}{Re}\left(\frac{\partial^2 V}{\partial X^2}+\frac{\partial^2 V}{\partial Y^2}\right) \tag{4}$$

Energy equation

$$\frac{\partial \theta}{\partial \tau}+U\frac{\partial \theta}{\partial X}+\left(V-\hat{V}\right)\frac{\partial \theta}{\partial Y}=\frac{1}{RePr}\left(\frac{\partial^2 \theta}{\partial X^2}+\frac{\partial^2 \theta}{\partial Y^2}\right). \tag{5}$$

Internal flow:

Continuity equation

$$\frac{\partial U_p}{\partial X}+\frac{\partial V_p}{\partial Y}=0 \tag{6}$$

Momentum equations

X direction

$$\begin{aligned}&\frac{\partial U_p}{\partial \tau}+U_p\frac{\partial\left(U_p/\varepsilon\right)}{\partial X}+\left(V_p-\varepsilon\hat{V}\right)\frac{\partial\left(U_p/\varepsilon\right)}{\partial Y}\\&=-\frac{\partial P_p}{\partial X}+\frac{1}{Re}\left(\frac{\partial^2 U_p}{\partial X^2}+\frac{\partial^2 U_p}{\partial Y^2}\right)-\frac{\varepsilon}{ReDa}U_p-\frac{F\varepsilon}{\sqrt{Da}}\left|\vec{U}_p\right|U_p\end{aligned} \tag{7}$$

Y direction

$$\begin{aligned}&\frac{\partial V_p}{\partial \tau}+U_p\frac{\partial\left(V_p/\varepsilon\right)}{\partial X}+\left(V_p-\varepsilon\hat{V}\right)\frac{\partial\left(V_p/\varepsilon\right)}{\partial Y}\\&=-\frac{\partial P_p}{\partial Y}+\frac{1}{Re}\left(\frac{\partial^2 V_p}{\partial X^2}+\frac{\partial^2 V_p}{\partial Y^2}\right)-\frac{\varepsilon}{ReDa}V_p-\frac{F\varepsilon}{\sqrt{Da}}\left|\vec{U}_p\right|V_p\end{aligned} \tag{8}$$

Energy equation

$$\frac{\partial \theta_p}{\partial \tau}+U_p\frac{\partial \theta_p}{\partial X}+\left(V_p-\varepsilon\hat{V}\right)\frac{\partial \theta_p}{\partial Y}=\frac{1}{RePr_e}\left(\frac{\partial^2 \theta_p}{\partial X^2}+\frac{\partial^2 \theta_p}{\partial Y^2}\right). \tag{9}$$

The above parameters of Da and F [10] are separately expressed as follows

$$Da=\frac{\varepsilon^3 D_p^2}{150(1-\varepsilon)^2} \tag{10}$$

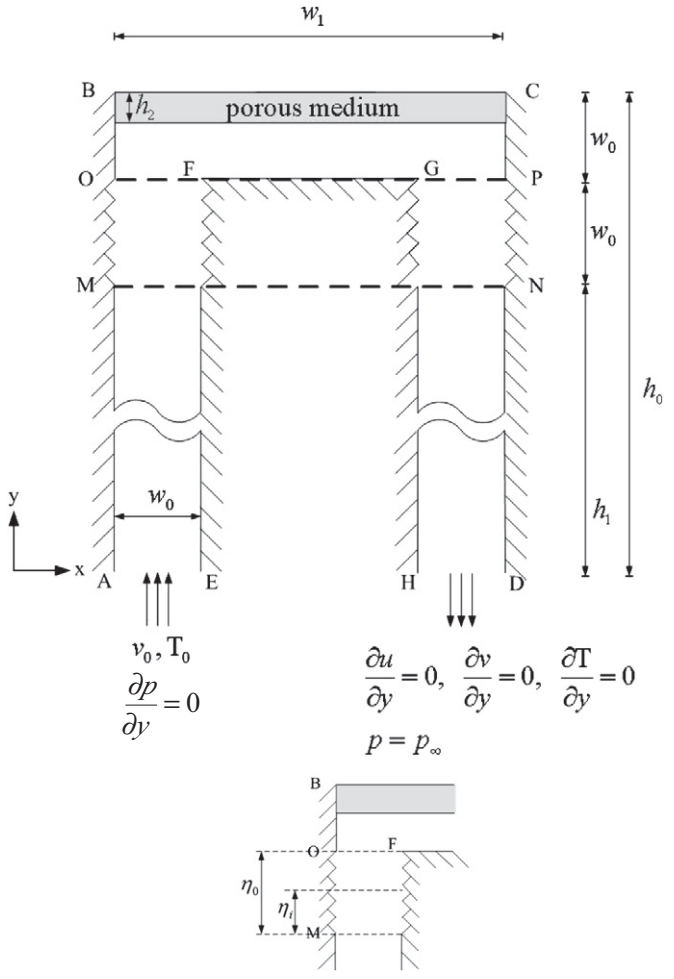


**Fig. 1.** Physical model.

$$F=\frac{1.75}{\sqrt{150}\varepsilon^{1.5}} \tag{11}$$

where $D_p$ is a dimensionless diameter of a copper bead. The other related parameters of the porous medium are obtained from [6].

In this study, the curved channel moves upward and downward in the vertical direction only, therefore, the horizontal mesh velocity is absent in the above governing equations. According to the ALE method, the mesh velocities are linearly distributed in the region between the $\overline{MN}$ (fixed) and $\overline{OP}$ (movable). In other regions, the mesh velocities are equal to 0. Steady state solutions are used as an initial condition before the channel executing reciprocating motion.

Boundary conditions of variables are indicated as follows, respectively.

At the inlet cross section $\overline{AE}$:

$$U=0, V=1, \frac{\partial P}{\partial Y}=0, \theta=0. \tag{12}$$

At the outlet cross section $\overline{HD}$:

$$\frac{\partial U}{\partial Y}=0, \frac{\partial V}{\partial Y}=0, \frac{\partial \theta}{\partial Y}=0, P=0. \tag{13}$$

Walls between the $\overline{MN}$ and $\overline{OP}$:

$$U=0, V=\begin{cases}0 & \tau=0\\ V_\eta & \tau>0\end{cases}, \frac{\partial P}{\partial X}=0, \frac{\partial \theta}{\partial X}=0. \tag{14}$$

Mesh velocities between the $\overline{MN}$ and $\overline{OP}$ are defined as $V_\eta = V_C \times \eta_i/\eta_0$, and is proportional to the distance between the $\overline{MN}$ and $\overline{OP}$.

Vertical walls $\overline{BO}$ and $\overline{CP}$:

$$U = 0, V = \begin{cases} 0 & \tau = 0 \\ V_C & \tau > 0 \end{cases}, \frac{\partial P}{\partial X} = 0, \frac{\partial \theta}{\partial X} = 0. \tag{15}$$

Horizontal wall $\overline{FG}$ and heated wall $\overline{BC}$:

$$\begin{cases} U = 0, V = \begin{cases} 0 & \tau = 0 \\ V_C & \tau > 0 \end{cases}, \frac{\partial P}{\partial Y} = 0, \frac{\partial \theta}{\partial Y} = 0 \\ U = 0, V = \begin{cases} 0 & \tau = 0 \\ V_C & \tau > 0 \end{cases}, \frac{\partial P}{\partial Y} = 0, \theta = 1 \end{cases} \tag{16}$$

Other walls:

$$U = 0, V = 0, \frac{\partial P}{\partial X} = 0, \frac{\partial \theta}{\partial X} = 0. \tag{17}$$

On the interface of the internal and external flows:

$$U = U_p, V = V_p, \theta = \theta_p, P = P_p$$
$$\frac{\partial U}{\partial t} = \frac{\partial U_p}{\partial t}, \frac{\partial V}{\partial t} = \frac{\partial V_p}{\partial t}, k_f \frac{\partial \theta}{\partial Y} = k_e \frac{\partial \theta_p}{\partial Y}. \tag{18}$$

## 3. Numerical method

Although the governing equations of the flow field are divided into two parts of the internal and external flows, the governing equations of both flows are the same forms except coefficients of the terms of the internal flow which can be obtained by empirical equations of an existing literature [10]. Then the same derived procedures of solution methods for governing equations of both flows can be used. The general procedures are exclusively derived as follows. As well, in order to calculate a pressure drop between the inlet and outlet of the channel, the method used in [36] is newly improved.

The governing equations are solved by the Galerkin finite element formulation and a backward scheme is adopted to deal with the time terms of the governing equations. In this study, a combination of eight-node quadratic Lagrangian interpolation for dealing with the velocity terms in the momentum and continuity equations, and four-node bilinear Lagrangian interpolation for treating the pressure terms are used. Then, Eqs. (2)–(4), and (6)–(8) can be expressed as the following matrix form

$$\sum_1^{ne} [D]^{(e)} \{\varphi\}^{(e)}_{\tau+\Delta\tau} = \sum_1^{ne} \left( [K_1]^{(e)} + [K_2]^{(e)} + [K_3]^{(e)} + [K_4]^{(e)} \right) \{\varphi\}^{(e)}_{\tau+\Delta\tau} = \sum_1^{ne} \{b\}^{(e)} \tag{19}$$

where

$$\{\varphi\}^{(e)}_{\tau+\Delta\tau} = \langle U_1, U_2, \ldots, U_8, V_1, V_2, \ldots, V_8, P_1, P_2, \ldots, P_4 \rangle^{m+1}_{\tau+\Delta\tau}. \tag{20}$$

$[K_1]^{(e)}$ includes the (m)th iteration values of U and V at the time $\tau + \Delta\tau$;
$[K_2]^{(e)}$ includes a shape function, diffusion terms, mesh velocity $\hat{V}$, time differential terms, and the Darcy resistance and inertia resistance adopted in Eqs. (7) and (8);
$[K_3]^{(e)}$ includes the pressure differential terms;
$[K_4]^{(e)}$ includes differential terms in the continuity equation;
$\{b\}^{(e)}$ includes the known values of U and V at the time $\tau$.

**Table 1**
Related length parameters of the physical model.

| Labels | $w_0/w_0$ | $w_1/w_0$ | $h_0/w_0$ | $h_1/w_0$ | $h_2/w_0$ |
|---|---|---|---|---|---|
| Relative length | 1 | 7 | 61 | 59 | 0.3 |

The energy Eqs. (5) and (9) can be expressed as the following matrix form

$$\sum_1^{ne} [Z]^{(e)} \{c\}^{(e)}_{\tau+\Delta\tau} = \sum_1^{ne} \left( [L_1]^{(e)} + [L_2]^{(e)} \right) \{c\}^{(e)}_{\tau+\Delta\tau} = \sum_1^{ne} \{f\}^{(e)} \tag{21}$$

where

$$\{c\}^{(e)}_{\tau+\Delta\tau} = \langle \theta_1, \theta_2, \ldots, \theta_8 \rangle_{\tau+\Delta\tau}. \tag{22}$$

$[L_1]^{(e)}$ includes the values of U and V at the time $\tau + \Delta\tau$;
$[L_2]^{(e)}$ includes a shape function, the mesh velocity $\hat{V}$, diffusion terms, and time differential terms;
$\{f\}^{(e)}$ includes the known values of $\theta$ at the time $\tau$.

The other detailed procedures of the solution method used in this work are the same as the solution method adopted in [37].

## 4. Results and discussion

Related lengths used in this study are tabulated in Table 1. Definitions of local and total Nusselt numbers, an enhancement of heat transfer rate *En* and a ratio index of driving forces *RP* are expressed as follows, respectively.

local Nusselt numbers

$$Nu_x = -\frac{\partial \theta}{\partial Y} \text{(without porous medium)} \tag{23}$$

$$Nu_{p,x} = -\frac{k_e}{k_f} \frac{\partial \theta_p}{\partial Y} \text{(porous medium)} \tag{24}$$

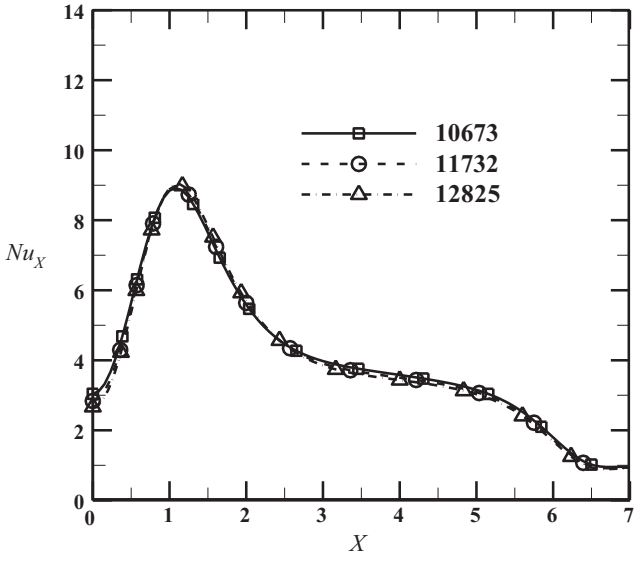


**Fig. 2.** Grid tests.

**Table 2**
Comparisons of average Nusselt numbers of existing [27] and present results.

| Da | Ra | Average Numbers | | | | | | | | |
|---|---|---|---|---|---|---|---|---|---|---|
| | | $\varepsilon = 0.4$ | | | $\varepsilon = 0.6$ | | | $\varepsilon = 0.9$ | | |
| | | [27] | Present results | Deviation (%) | [27] | Present results | Deviation (%) | [27] | Present results | Deviation (%) |
| $10^{-4}$ | $10^5$ | 1.067 | 1.064 | 0.28 | 1.071 | 1.067 | 0.37 | 1.072 | 1.069 | 0.28 |
| | $10^6$ | 2.55 | 2.594 | 1.73 | 2.725 | 2.701 | 0.88 | 2.740 | 2.785 | 1.64 |
| $10^{-2}$ | $10^3$ | 1.01 | 1.008 | 0.2 | 1.015 | 1.012 | 0.3 | 1.023 | 1.018 | 0.49 |
| | $10^4$ | 1.408 | 1.360 | 3.41 | 1.530 | 1.491 | 2.55 | 1.64 | 1.631 | 0.55 |

total Nusselt numbers

$$\overline{Nu}_x = \int_0^{W_1} Nu_x dX \tag{25}$$

$$\overline{Nu}_{p,x} = \int_0^{W_1} Nu_{p,x} dX \tag{26}$$

$$En = \frac{\overline{Nu}_{p,x} - \overline{Nu}_x}{\overline{Nu}_x} \tag{27}$$

$$\Delta P = P_{(\text{inlet},\overline{AE})} - P_{(\text{outlet},\overline{HD})} \tag{28}$$

$$RP = \frac{\Delta P_{\varepsilon \neq 0} - \Delta P_{\text{without porous medium}}}{\Delta P_{\text{without porous medium}}}. \tag{29}$$

Results of grid tests are shown in Fig. 2. According to numerical tests, total elements and nodes are 11,732 and 36,901, respectively. Numbers of elements and nodes used in the porous medium and without porous medium regions are (392, 1981) and (11,340, 35,520), respectively, and the time step $\Delta\tau = {}^{1}/_{(56F_C)}$ is chosen for all situations.

In Table 2, comparisons of average Nusselt numbers of the existing study [27], in which a cavity with constant porosity medium was regarded as the physical model, and the present study, in which the

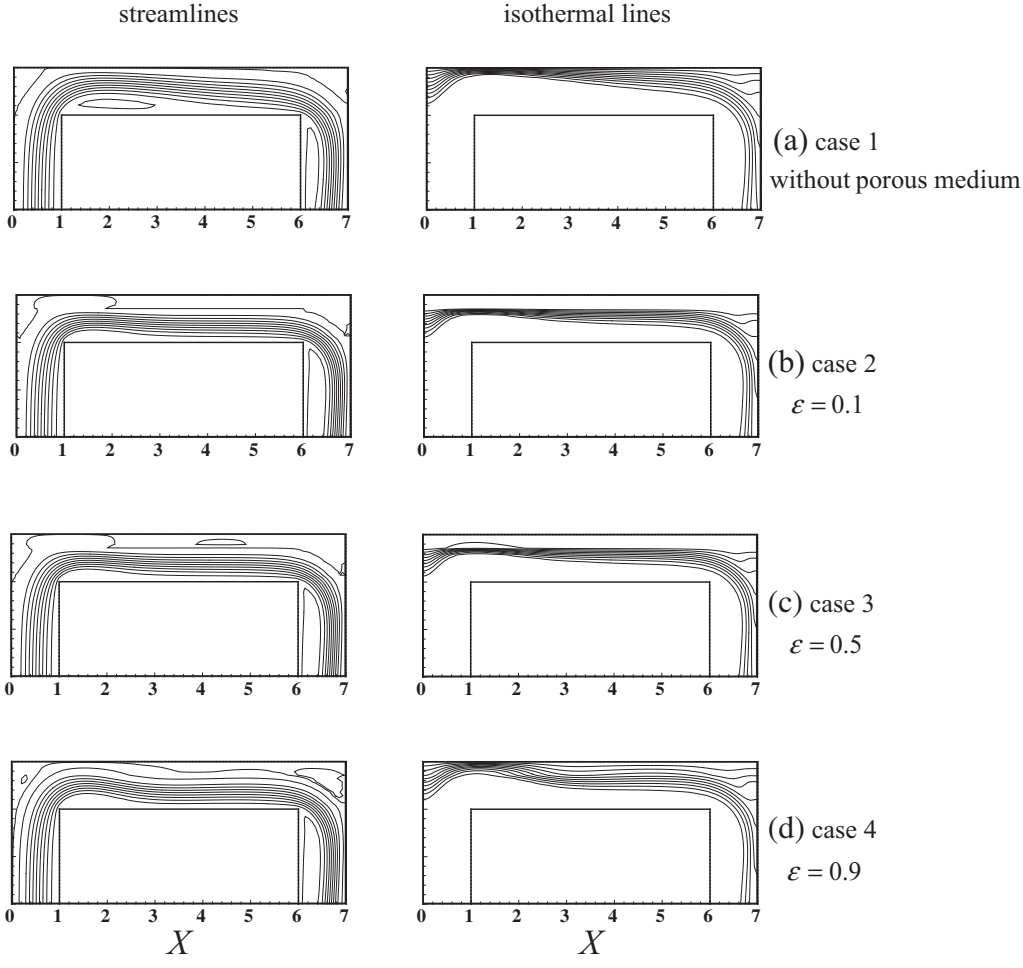


**Fig. 3.** Comparisons of distributions of streamlines and isothermal lines for cases of 1–4 at a stationary situation under Re = 200.

physical model is newly modified to match that of [27], are indicated. Two different methods of a finite difference scheme [27] and a finite element scheme used in the work are adopted. Then slight deviations exist between two results.

In Fig. 3, distributions of streamlines and isothermal lines of different porosities at a stationary state are indicated, respectively. Under the without porous medium situation, a dense distribution of isothermal lines caused by an impingement of cooling fluids from the left vertical channel is observed in the left region of the top surface. Afterward, the behavior of rebound of cooling fluids revealed by the indication of the distribution of streamlines occurs, and finally cooling fluids turn flowing directions to the right vertical channel in advance. This phenomenon is rather inferior to heat transfer rates of the back region of the top surface. Under situations of $\varepsilon = 0.1$ and 0.5, the porous medium is dense and similar to a solid heat dissipation plate. Via heat conduction mode, the temperatures distributed on the interface between the regions of porous medium and without porous medium are slightly smaller than that assigned on the heat top surface. These phenomena are indicated by the distributions of isothermal lines shown in Fig. 3(b) and (c). Then convective heat transfer mechanisms mainly occur on the interface instead of the heat top surface. Then, the space for cooling fluids flowing through the horizontal channel is contracted, and velocities of cooling fluids are accelerated. The behavior of the rebound is then weakened, and cooling fluids relatively do not turn flowing directions to the right vertical channel in advance. Due to the impingement caused by cooling fluids from the left vertical channel, dense distributions of isothermal lines are observed in the left region. As well, cooling fluids are slightly scattered by the porous medium when cooling fluids impinge on the porous medium that causes the regions of dense distributions of isothermal lines of Fig. 3(b) and (c) to be slightly wider than that of Fig. 3(a). As for the situation of $\varepsilon = 0.9$, the sparse arrangement of porous medium results in distributions of streamlines and isothermal lines being similar to those of the situation of without porous medium. The rebound of cooling fluids occurs in the porous medium neighboring the impinging region that leads rebounding fluids to be impeded by the porous medium and difficultly to flow along the heat top surface again. These mechanisms are rather inferior to those of the without porous medium situation for heat transfer rates.

Usually, the larger the porosity is, the sparser the porous medium becomes. A pressure drop obtained by the pressure difference between the inlet and outlet can be regarded as an index of the strength of driving force. As a result, under the same Reynolds number the larger the porosity is, the smaller the pressure drop becomes.

In Fig. 4, distributions of local Nusselt numbers of different porosities under a stationary state are indicated, respectively. In the previous study [36], porous medium was not installed on the heat surface, and the maximum local Nusselt number on the left region was obtained by the impingement of cooling fluids from the left vertical channel. After the location of rebound, cooling fluids start to turn flowing directions to the right vertical channel that causes the distribution of local Nusselt numbers to decrease severely. In the situation of $\varepsilon = 0.1$ as shown in Fig. 4(a), the stronger strength of the driving force indicated by the magnitude of *RP* causes cooling fluids to achieve the maximum local Nusselt number which is larger than that of the situation of without porous medium. Also, the region around the maximum local Nusselt number is wider than that of the situation of without porous medium because of the scattering effect of the porous medium mentioned above. Due to the contraction of the horizontal channel mentioned above, cooling fluids are accelerated to flow through the horizontal channel that leads the distribution of local Nusselt numbers to be enhanced relative to the situation without porous medium in the right part of the middle region. The total enhancement revealed by the magnitude of *En* is about 20%. Phenomena of the situation of $\varepsilon = 0.5$ shown in Fig. 4(b) are similar to those of the situation of $\varepsilon = 0.1$, and then the distribution of local Nusselt numbers is also similar to that of the situation of $\varepsilon = 0.1$. The strength of the driving force is slightly smaller than

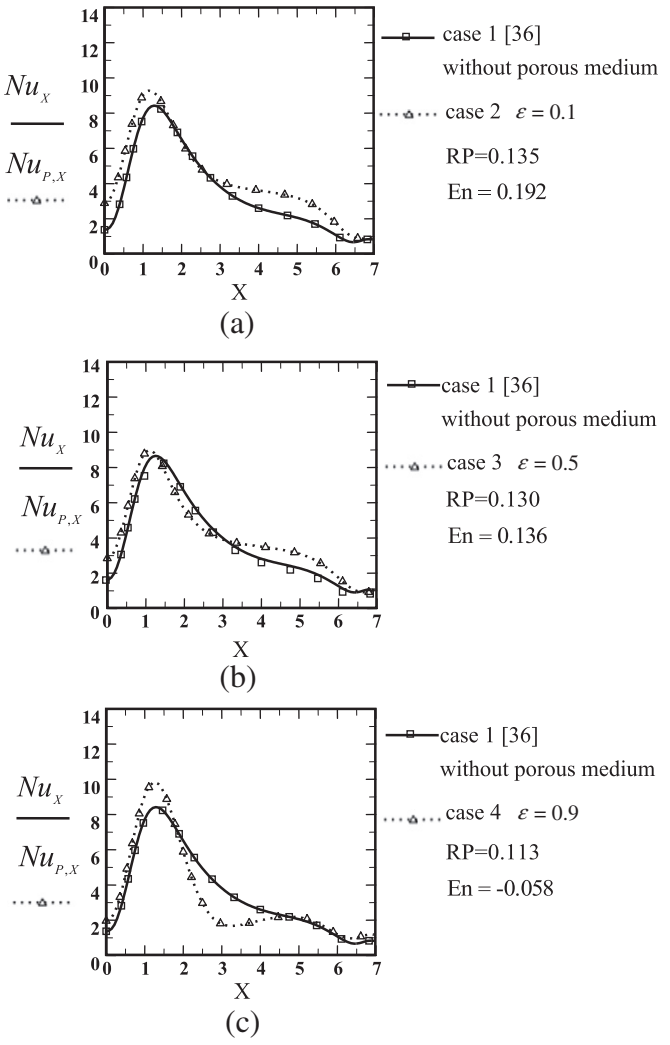


**Fig. 4.** Distributions of local Nusselt numbers for different porosities at a stationary situation under Re = 200.

that of the situation of $\varepsilon = 0.1$. The total enhancement is about 14% which is reasonable. In Fig. 4(c), the porosity is sparse and the porous medium is not appropriately regarded as a solid heat dissipation plate like the above situations, and then cooling fluids are able to penetrate the porous medium and obtain the larger local Nusselt number on the impinging location. After the occurrence of the rebound behavior, cooling fluids are impeded by the porous medium and difficultly flows along the heat top surface again that directly deteriorates the distribution of local Nusselt numbers. As a result, the total enhancement, which is about −6%, is severely decreased and even smaller than the situation without porous medium.

In Fig. 5, distributions of local Nusselt numbers of situations of cases of 1 and 3 within one periodic cycle are indicated, respectively. The signal "↑" means the moving direction of the curved channel. Shown in Fig. 5(a), the channel is at a status of the maximum upward velocity and the space of the channel is being enlarged. The channel is able to absorb more upward cooling fluids which directly impinge on the top surface, and then a remarkable enhancement, which is even larger than the enhancement shown in Fig. 4(b), is achieved. In Fig. 5(b), the channel stops at the highest location of movement and the space of the channel is no longer enlarged. Naturally, the enhancement is decreased rapidly. In Fig. 5(c), the channel is under a status of the maximum downward

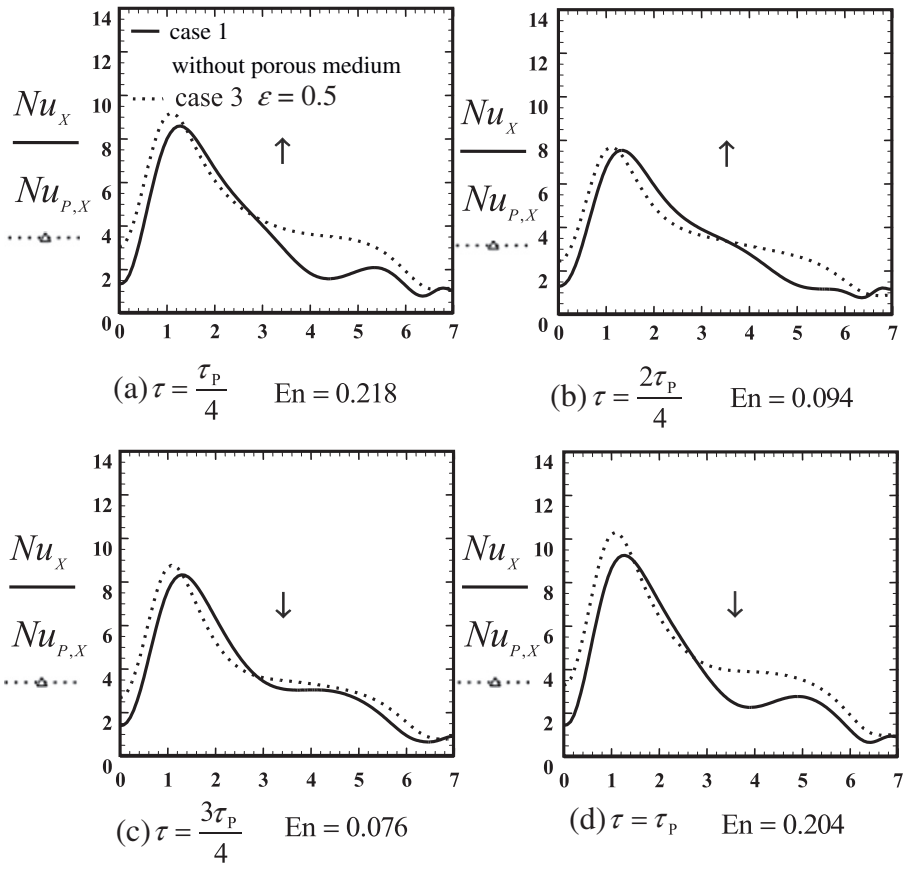


**Fig. 5.** Distributions of local Nusselt numbers for cases of 1 and 3 within one periodic cycle under Re = 200, $L_c$ = 0.25, and $F_C$ = 0.1 situation.

velocity, and the space of the channel is being contracted. The downward impulse of the channel severely compels upward cooling fluids from the left vertical channel to turn their flowing directions to the right vertical channel. This behavior is certainly injurious to the enhancement of heat transfer rates of the top surface. In Fig. 5(d), the channel stops at the lowest location and prepares for the next upward movement. Detrimental factors mentioned above vanish and the enhancement naturally recovers. The enhancement or deterioration of the heat transfer rates caused by the porous medium mainly occurs in the right part of the middle region as shown in the above figures, because the effects of the porous medium on the maximum local Nusselt number caused by the impingement of cooling fluids and the minimum local Nusselt number distributed in the corner are slight.

Related variables and comparisons of effects of different parameters on the enhancement are tabulated in Table 3, respectively. In cases of 5–8, under a situation of a low Reynolds number (Re = 200) and small magnitudes of the $L_c$ = 0.25 and $F_C$ (=0.1), the trend of results of enhancements is similar to the situation of stationary state indicated in cases of 1–4. The reasons are mentioned above. Tabulated in cases of 9–12, the frequency $F_C$ is increased to 0.4 which directly causes the velocity of the channel $V_m$ to be increased. Doubtlessly, remarkable enhancements are achieved, even the enhancement of the situation of $\varepsilon$ = 0.9 becomes positive. Tabulated in cases of 13–16, the magnitude of Reynolds number is broadly increased to 750. The driving force becomes stronger that causes cooling fluids of the situation of $\varepsilon$ = 0.5 to be able to penetrate the porous medium. These phenomena are similar to those of the situation of the Reynolds number of 200 and the porosity of 0.9 mentioned above. Although the magnitudes of average Nusselt numbers of cases of 15 and 16 are increased, the magnitudes of enhancements unexpectedly become negative.

## 5. Conclusions

An investigation of the enhancement of forced convection of the reciprocating curved channel by the porous medium is conducted numerically. In order to achieve the enhancement of heat transfer rates, careful

**Table 3**
Comparisons of average Nusselt numbers and enhancements of different parameters under a stationary and reciprocating motions.

| $\varepsilon$ | $D_p$ | Da by Eq. (10) |
|---|---|---|
| 0.1 | 0.1 | $8.23 \times 10^{-8}$ |
| 0.5 | 0.1 | $3.33 \times 10^{-5}$ |
| 0.9 | 0.1 | $4.86 \times 10^{-3}$ |

| Case | $\varepsilon$ | Re | $L_c$ | $F_C$ | $V_m$ | $\overline{Nu}$ | *En* |
|---|---|---|---|---|---|---|---|
| 1 | Without porous medium | 200 | – | – | – | 1.78 | 0 |
| 2 | 0.1 | 200 | – | – | – | 2.13 | 0.20 |
| 3 | 0.5 | 200 | – | – | – | 2.03 | 0.14 |
| 4 | 0.9 | 200 | – | – | – | 1.68 | −0.06 |
| 5 | Without porous medium | 200 | 0.25 | 0.1 | 0.157 | 3.58 | 0 |
| 6 | 0.1 | 200 | 0.25 | 0.1 | 0.157 | 4.27 | 0.19 |
| 7 | 0.5 | 200 | 0.25 | 0.1 | 0.157 | 4.07 | 0.14 |
| 8 | 0.9 | 200 | 0.25 | 0.1 | 0.157 | 3.38 | −0.06 |
| 9 | Without porous medium | 200 | 0.25 | 0.4 | 0.628 | 4.06 | 0 |
| 10 | 0.1 | 200 | 0.25 | 0.4 | 0.628 | 4.73 | 0.17 |
| 11 | 0.5 | 200 | 0.25 | 0.4 | 0.628 | 4.52 | 0.11 |
| 12 | 0.9 | 200 | 0.25 | 0.4 | 0.628 | 4.32 | 0.06 |
| 13 | Without porous medium | 750 | 0.25 | 0.1 | 0.157 | 7.20 | 0 |
| 14 | 0.1 | 750 | 0.25 | 0.1 | 0.157 | 7.85 | 0.09 |
| 15 | 0.5 | 750 | 0.25 | 0.1 | 0.157 | 6.99 | −0.03 |
| 16 | 0.9 | 750 | 0.25 | 0.1 | 0.157 | 6.70 | −0.07 |

considerations of the porous medium for different flow conditions are necessary. Several conclusions are drawn as follows.

1. A situation of the small porosity and strong driving force usually achieves the enhancement of heat transfer rates of the reciprocating curved channel.
2. Cooling fluids are easily impeded in the porous medium with a high porosity. Those behaviors are inferior to heat transfer mechanisms.
3. A situation of the short amplitude and large frequency often gains an achievement.
4. Enhancements of the heat transfer rates are mainly concentrated in the right part of the middle region.

## Acknowledgment

The authors gratefully acknowledge the support of the Natural Science Council Taiwan, ROC under Contact NSC 97-2221-E-009-144-MY2.

## References

[1] J.C.Y. Koh, R. Colony, Analysis of cooling effectiveness for porous material in a coolant passage, ASME J. Heat Transf. (August 1974) 324–330.
[2] J.C.Y. Koh, R.L. Stevens, Enhancement of cooling effectiveness by porous materials in coolant passage, J. Heat Transf. (1975) 309–311.
[3] J.C. Han, Heat transfer and friction in channels with two opposite Rib-roughed walls, ASME J. Heat Transf. 106 (1984) 774–781.
[4] K. Vafai, C.L. Tien, Boundary and inertia effects on flow and heat transfer in porous media, Int. J. Heat Mass Transf. 24 (1981) 195–203.
[5] M. Kaviany, Laminar flow through a porous channel bounded by isothermal parallel plates, Int. J. Heat Mass Transf. 28 (1985) 851–858.
[6] K. Vafai, Convective flow and heat transfer in variable-porosity media, J. Fluid Mech. 147 (1984) 233–259.
[7] K. Vafai, R.L. Alkire, C.L. Tien, An experimental investigation of heat transfer in variable porosity media, J. Heat Transf. 107 (1985) 642–647.
[8] P. Cheng, C.T. Hsu, Fully-developed forced convective flow through an annular packed-sphere bed with wall effects, Int. J. Heat Mass Transf. 29 (1986) 1843–1853.
[9] P. Cheng, C.T. Hsu, Applications of Van Driest's mixing length theory to transverse thermal dispersion in a packed-bed with boundary walls, Int. Commun. Heat Mass Transf. 13 (1986) 613–625.
[10] W.S. Fu, H.C. Huang, Thermal performances of different shapes of porous blocks under an impinging jet, Int. J. Heat Mass Transf. 40 (1997) 2261–2272.
[11] A.A. Mohamad, Heat transfer enhancements in heat exchangers fitted with porous media. Part I: constant wall temperature, Int. J. Therm. Sci. 42 (2003) 385–395.
[12] M.M. Nandeppanavar, M.S. Abel, M.N. Siddalingappa, Heat transfer through a porous medium over a stretching sheet with effect of viscous dissipation, Chem. Eng. Commun. 200 (2013) 1513–1529.
[13] M.M. Rashidi, S.A. Mohimanian Pour, T. Hayat, S. Obaidat, Analytic approximate solutions for steady flow over a rotating disk in porous medium with heat transfer by homotopy analysis method, Comput. Fluids 54 (2012) 1–9.
[14] D.A. Nield, A.V. Kuznetsov, Optimization of forced convection heat transfer in a composite porous medium channel, Transp. Porous Media 99 (2013) 349–357.
[15] N.I Eldabe, M.A. Zeid, Thermal diffusion and diffusion thermo effects on the viscous fluid flow with heat and mass transfer through porous medium over a shrinking sheet, J. Appl. Math. 2013 (2013) p. 11.
[16] M.A. Combarnous, P. Bia, Combined free and forced convection in porous medium, Soc. Pet. Eng. J. 11 (1971) 399–405.
[17] M. Haajizadeh, C.L. Tien, Combined free and forced convection in a horizontal porous channel, Int. J. Heat Mass Transf. 27 (1984) 799–813.
[18] V. Prasad, F.C. Lai, F.A. Kulacki, Mixed convection in horizontal porous layers heated from below, ASME J. Heat Transf. 110 (1988) 395–402.
[19] F.C. Chou, C.J. Chen, W.Y. Lien, Analysis and experiment of non-Darcian convection in horizontal square packed-sphere channels — part 2: mixed convection, Int. J. Heat Mass Transf. 35 (1992) 1197–1207.
[20] S. Mukhopadhyay, Effect of thermal radiation on unsteady mixed convection flow and heat transfer over a porous stretching surface in porous medium, Int. J. Heat Mass Transf. 52 (2009) 3261–3265.
[21] P. Cheng, W.J. Minkowycz, Free convection about a vertical flat plate embedded in a porous medium with application to heat transfer from a dike, J. Geophys. Res. 82 (1977) 2040–2044.
[22] O.V. Trevisan, A. Bejan, Natural convection with combined heat and mass transfer buoyancy effects in a porous medium, Int. J. Heat Mass Transf. 28 (1985) 1597–1611.
[23] F.C. Lai, F.A. Kulacki, Coupled heat and mass transfer by natural convection from vertical surfaces in porous media, Int. J. Heat Mass Transf. 34 (1991) 1189–1194.
[24] S.W. Hsiao, P. Cheng, C.K. Chen, Non-uniform porosity and thermal dispersion effects on natural convection about a heated horizontal cylinder in an enclosed porous medium, Int. J. Heat Mass Transf. 35 (1992) 3407–3418.
[25] F. Alavyoon, On natural convection in vertical porous enclosures due to prescribed fluxes of heat and mass at the vertical boundaries, Int. J. Heat Mass Transf. 36 (1993) 2479–2498.
[26] B.I. Pavel, A.A. Mohamad, An experimental and numerical study on heat transfer enhancement for gas heat exchangers fitted with porous media, Int. J. Heat Mass Transf. 47 (2004) 4939–4952.
[27] P. Nithiarasu, K.N. Seetharamu, T. Sundararajan, Natural convective heat transfer in a fluid saturated variable porosity medium, Int. J. Heat Mass Transf. 40 (1997) 3955–3967.
[28] D.A. Nield, A.V. Kuznetsov, The Cheng–Minkowycz problem for natural convective boundary layer flow in a porous medium saturated by a nanofluid, Int. J. Heat Mass Transf. 52 (2009) 5792–5795.
[29] A.V. Kuznetsov, D.A. Nield, The Cheng–Minkowycz problem for natural convective boundary layer flow in a porous medium saturated by a nanofluid: a revised model, Int. J. Heat Mass Transf. 65 (2013) 682–685.
[30] W.S. Fu, W.W. Ke, Natural convection in a porous medium enclosure with evaporation and condensation, J. CSME 20 (2000) 563–573.
[31] C.P. Chiu, Y.S. Kuo, Study of turbulent heat transfer in reciprocating engine using as algebraic grid generation technique, Numer. Heat Transf. A 27 (1995) 255–271.
[32] S.W. Chang, L.M. Su, Influence of reciprocating motion on heat transfer inside a ribbed duct with application to piston cooling in marine diesel engines, J. Ship Res. 41 (1997) 332–339.
[33] S.W. Chang, L.M. Su, Heat transfer in a reciprocating duct fitted with transverse ribs, Exp. Heat Transf. 12 (1999) 95–115.
[34] C.H. Cheng, C.K. Hung, Numerical predictions of flow thermal fields in a reciprocating piston-cylinder assembly, Numer. Heat Transf. A 38 (2000) 397–421.
[35] S.W. Chang, L.M. Su, W.D. Morris, T.M. Liou, Heat transfer in a smooth-walled reciprocating anti-gravity open thermosyphon, Int. J. Heat Mass Transf. 42 (2003) 1089–1103.
[36] W.S. Fu, S.H. Lian, Y.H. Liao, An investigation of heat transfer of a reciprocating piston, Int. J. Heat Mass Transf. 49 (2006) 4360–4371.
[37] W.S. Fu, Y.C. Lai, S.H. Huang, An enhancement of the back region forced convection heat transfer rates of a reciprocating curved channel with a rib by the ALE method, Int. Commun. Heat Mass Transf. 49 (2013) 41–48.